SCIENCE CHINA
Information Sciences

• RESEARCH PAPER •

October 2020, Vol. 63 202501:1–202501:15
https://doi.org/10.1007/s11432-019-2689-4

Effect on ion-trap quantum computers from the quantum nature of the driving field

Biyao YANG[1,2,3,4] & Li YANG[1,3*]

[1]*State Key Laboratory of Information Security, Institute of Information Engineering, Chinese Academy of Sciences, Beijing* 100049*, China;*
[2]*State Key Laboratory of Cryptology, P.O. Box* 5159*, Beijing* 100878*, China;*
[3]*School of Cyber Security, University of Chinese Academy of Sciences, Beijing* 100093*, China;*
[4]*Beijing Institute of Information Application Technology, Beijing* 100044*, China*

Received 20 April 2019/Revised 15 July 2019/Accepted 22 September 2019/Published online 18 May 2020

Abstract In this study, we evaluate the effect on ion-trap quantum computers (QCs) from the quantum nature of the driving field, and propose a theoretical limit for ion-trap QCs that may impact the design of quantum algorithms and realization of practical QCs. We obtain, for the first time, the permitted depth of logical operation for fault-tolerant ion-trap QCs. Physically, we provide an exact (full-quantum) description of the QC system, and present for the first time its time evolution after gate operations; mathematically, we solve problems such as certain summations of trigonometric series with any given precision. Comparing the actual state after CNOT gates driven by a quantized field with the expected state, we obtain the failure probability and estimate that the number of CNOT gates on the same pair of physical qubits is not more than 10^2 in one error-correction period, which is a physical limit that cannot be easily overcome. The conclusion can help determine the number of CNOT operations between coding and decoding in one error-correction period and can be used as a reference for quantum algorithm design.

Keywords quantum computing, ion-trap, quantum algorithm, fault-tolerant quantum computation, threshold theorem, permitted depth of logical operation

Citation Yang B Y, Yang L. Effect on ion-trap quantum computers from the quantum nature of the driving field. Sci China Inf Sci, 2020, 63(10): 202501, https://doi.org/10.1007/s11432-019-2689-4

1 Introduction

Quantum computers (QCs) can dramatically speed up some tasks compared to classical computers [1–5]. One application of QCs is to break the cryptosystems currently in use such as the RSA [6] and ElGamal [7]. Many quantum-computing processors have been designed, and the ion-trap QC proposed by Cirac and Zoller [8] is one of the two leading ones (the other is superconducting QC). Ion-trap QCs have a small decoherence rate, and have experimentally outperformed superconducting QCs with better qubit connectivity [9]. Researchers on ion-trap QCs have made great progress in the recent years: there have been many advances toward scalable QCs [10–14], high-fidelity gates (including the universal quantum gate set) have been demonstrated [15–18], a scalable Shor algorithm has been realized on ion-trap QCs with more than 10 qubits [19].

However, there exists a theoretical issue related to the ion-trap quantum processor. This type of QCs are driven by coherent fields (such as laser fields), and the fields are considered classical in the original proposal [8]; whereas, actually, the field is a quantum system. The quantum state of laser field is the

* Corresponding author (email: yangli@iie.ac.cn)

coherent state $|\psi\rangle = \sum_{n=0}^{\infty} c_n|n\rangle$ (with $|c_n|^2 = \frac{\mathrm{e}^{-\bar{n}}\bar{n}^n}{n!}$), which has various number-state components $|n\rangle$ $(n = 0, 1, \ldots, \infty)$. The dynamics of ion qubits driving by a coherent state is different from that driving by a planar wave of a classical laser field. However, the operations needed to implement the Cirac-Zoller CNOT gate are given from the evolution of a laser-atom system under classical laser field [8]. As the system obeys quantum rules, when the operations in [8] are applied to ion qubits, the actual operation result may be different from the expected one, resulting in error. After repeated operations, the error becomes relatively large. When the error goes beyond the threshold of fault-tolerant quantum computation, it poses a great challenge for the realization of practical QCs.

Based on this, some researchers have considered the quantum nature of the driving fields [20,21]. Their solution was to add quantum fluctuations to the classical treatment of the laser fields, without considering its effects on quantum computation or on the realization of quantum algorithms. However, in the case of ion-trap QCs, in which each two-level system undergoes quantum oscillations driven by pulse trains [22], there exist phenomena that cannot be predicted by simply adding quantum fluctuations to a semiclassical method; a more accurate full-quantum treatment [22, 23] is needed.

The difficulties with full-quantum treatment lie in two aspects: providing an exact description of the QC system and its time-evolution after many gate operations (physically), and solving problems such as certain summations of trigonometric series with any given precision (mathematically). In [22], the Rabi oscillation of a two-level system driven by a quantized pulse train, an application of which was QCs driven by the coherent field mentioned above, was studied. As a result, a model was developed to deal with the two-level system, an algorithm was proposed to calculate the summation with any given precision, some meaningful results of this basic physical interaction were obtained, and a parameter called the permitted depth of logical operation was derived. The parameter limited the operation number on any physical qubit in quantum processors and described the property of a physical realization scheme of QCs.

The study reported in [22] prepared the foundations for this paper. We studied the permitted depth of logical operation for the ion-trap QCs in this study, focusing on the controlled-NOT (CNOT) operation. The CNOT gate can be considered as the key to the realization of a QC, because it, together with the single-qubit gate, gives a universal set of QCs [24]. Moreover, the computational complexity of an algorithm can be reduced to the number of CNOT gates [25]. We calculate the failure probability after CNOT operations and propose the permitted depth of logical operation for the ion-trap QCs.

The remainder of this paper is organized as follows. In Section 2, we present some preliminaries, upon which further discussion is based. In Section 3, we obtain the states of the qubit states after one CNOT gate driven by a quantized field, and the time evolution after many CNOT operations are calculated. In Section 4, a theoretical limit (permitted depth of logical operation) of an ion-trap QC is given, based on the failure probability derived. In Section 5, we present the discussion. In Section 6, the conclusion from our research is provided.

2 Preliminaries

2.1 Cirac-Zoller CNOT gate

The CNOT gate together with single-qubit gates are universal for quantum computation. It has two input qubits known as the control qubit and the target qubit, respectively. The function of the CNOT gate is to flip the state of the target bit conditioned on the state of the control bit.

The CNOT gate can be seen as the key to the realization of QCs: besides it forms a universal set for quantum computation together with single-qubit gates, the computation complexity of an algorithm can be reduced to the number of CNOT gates [25]. Consider the CNOT gate in ion-trap QCs. There are mainly three CNOT schemes for the ion-trap QC, namely the Cirac-Zoller CNOT gate proposed in the original paper [8], the geometrical phase gate [26], and Mϕlmer-Sϕrensen gate [27]. For schemes other than the Cirac-Zoller CNOT gate, despite their advantages, there are some shortcomings; for example, they experience difficulty while operating on a given qubit in the ion string; they need other techniques to cancel the effect on other ions, and it is not very convenient to construct quantum algorithms from

globally acting entangling operations [28]. Consequently, the Cirac-Zoller CNOT gate is widely adopted for the implementation of QCs.

The implementation process of the Cirac-Zoller CNOT gate is from the following evolution in ion-trap QCs, which is based on the classical treatment of laser fields [8].

• Carrier transition where the laser's frequency ω equals the internal transition frequency of the ion ω_0. Laser polarization $q = 0$, and the equilibrium position of the ion coinciding with the antinode of the laser standing wave (the traveling wave can also be used), for an interaction time $t = k\pi/\Omega$ (i.e., using a $k\pi$ pulse, here Ω is Rabi frequency), the process is described using the following unitary evolution operator:

$$V_n^k(\phi) = \exp\left[-\mathrm{i}k\frac{\pi}{2}(|1\rangle_n\langle 0|\mathrm{e}^{-\mathrm{i}\phi} + \mathrm{h.c.})\right], \tag{1}$$

where ϕ is the laser phase, $|1\rangle_n$ and $|0\rangle_n$ denotes the upper (lower) level of nth ion, h.c. denotes hermitian conjugate. Then

$$\begin{aligned} |0\rangle_n &\to \cos(k\pi/2)|0\rangle_n - \mathrm{i}\mathrm{e}^{\mathrm{i}\phi}\sin(k\pi/2)|1\rangle_n, \\ |1\rangle_n &\to \cos(k\pi/2)|1\rangle_n - \mathrm{i}\mathrm{e}^{-\mathrm{i}\phi}\sin(k\pi/2)|0\rangle_n. \end{aligned} \tag{2}$$

• Red sideband transition where the laser's frequency detuning equals minus the center-of-mass (CM) mode frequency ω_{t}. Laser polarization $q = 0$, and the equilibrium position of the ion coinciding with the node of the laser standing wave, for an interaction time $t = k\pi/(\Omega\eta/\sqrt{N})$ (i.e., using a $k\pi$ pulse, here η is the Lamb-Dick parameter and N is the number of ions), the process is described by the following unitary evolution operator:

$$U_n^k(\phi) = \exp\left[-\mathrm{i}k\frac{\pi}{2}(|1\rangle_n\langle 0|b\mathrm{e}^{-\mathrm{i}\phi} + \mathrm{h.c.})\right], \tag{3}$$

where $b^\dagger$ and b are the creation and annihilation operators of phonons, respectively. Then,

$$\begin{aligned} |0\rangle_n|1\rangle_{\mathrm{ph}} &\to \cos(k\pi/2)|0\rangle_n|1\rangle_{\mathrm{ph}} - \mathrm{i}\mathrm{e}^{\mathrm{i}\phi}\sin(k\pi/2)|1\rangle_n|0\rangle_{\mathrm{ph}}, \\ |1\rangle_n|0\rangle_{\mathrm{ph}} &\to \cos(k\pi/2)|1\rangle_n|0\rangle_{\mathrm{ph}} - \mathrm{i}\mathrm{e}^{-\mathrm{i}\phi}\sin(k\pi/2)|0\rangle_n|1\rangle_{\mathrm{ph}}, \end{aligned} \tag{4}$$

where the subscript ph denotes phonons.

Suppose the xth ion is the control qubit and the yth ion is the target qubit. According to [8], the five steps to implement CNOT gate are (a simple example is shown later) as follows.

Step 1. Carrier transition of the yth ion (Eq. (1) applicable). Apply a $\pi/2$ pulse to the yth ion. The laser phase is $\phi = -\pi/2$. This rotates the state of the yth ion only.

Step 2. Red sideband transition of the xth ion (Eq. (3) applicable). Apply a π pulse to the xth ion, $\phi = 0$. This maps the internal state of the xth ion to the motion of the ion string (phonons).

Step 3. Red sideband transition of the yth ion (Eq. (3) applicable). Apply a 2π pulse to the yth ion. $\omega = \omega' - \omega_{\mathrm{t}}$, where ω' is the frequency difference between the ground state $|0\rangle$ and the auxiliary state $|\mathrm{aux}\rangle$, and $\phi = 0$. This changes the sign of the target ion (the yth ion) conditioned on the motion of the ion string.

Step 4. The same as Step 2. This maps the motion of the ion string back onto the original ion.

Step 5. Carrier transition of the yth ion (Eq. (1) applicable). Apply a $\pi/2$ pulse to the yth ion, $\phi = \pi/2$. This rotates the state of the yth ion only.

If the initial state is $|1\rangle_x|0\rangle_y$, the state evolution is as follows:

$$\begin{aligned} |1\rangle_x|0\rangle_y|0\rangle_{\mathrm{ph}} &\xrightarrow{\text{Step 1}} |1\rangle_x\frac{1}{\sqrt{2}}(|0\rangle_y - |1\rangle_y)|0\rangle_{\mathrm{ph}} \\ &\xrightarrow{\text{Step 2}} -\frac{\mathrm{i}}{\sqrt{2}}|0\rangle_x(|0\rangle_y - |1\rangle_y)|1\rangle_{\mathrm{ph}} \\ &\xrightarrow{\text{Step 3}} \frac{\mathrm{i}}{\sqrt{2}}|0\rangle_x(|0\rangle_y + |1\rangle_y)|1\rangle_{\mathrm{ph}} \\ &\xrightarrow{\text{Step 4}} \frac{1}{\sqrt{2}}|1\rangle_x(|0\rangle_y + |1\rangle_y)|0\rangle_{\mathrm{ph}} \\ &\xrightarrow{\text{Step 5}} |1\rangle_x|1\rangle_y|0\rangle_{\mathrm{ph}}. \end{aligned} \tag{5}$$

2.2 Fault-tolerant quantum computation

Fault-tolerant quantum computation (FTQC) makes the long processing of quantum information feasible. In FTQC, each qubit in the original circuit is replaced with an encoded block of qubits, using an error-correcting code, and each gate in the original circuit is replaced with an fault-tolerant gate acting on the encoded state. By performing error-correction periodically on the encoded state, we can prevent the accumulation of errors in the state.

Fault-tolerant error-correction and concatenated codes are important elements in FTQC. Quantum error-correction networks are themselves non-trivial quantum networks where errors can occur during their performance. Fault-tolerant error-correction supplies fault-tolerant ancillas, verification of the ancilla state, testing of syndrome measurements, among others, to ensure reliable error-correction [29]. The construction based on concatenated codes can be used to reduce the effective error rate achieved by the computation further. Suppose the error-correction code can correct one-qubit error, we simulate a circuit containing $p(n)$ gates, where n is the size of some problem, to achieve a final accuracy of ϵ, each gate in the circuit must be accurate to $\epsilon/p(n)$; thus, the concatenate number k should satisfy [24, 30]

$$\frac{(cp)^{2^k}}{c} \leqslant \frac{\epsilon}{p(n)}. \tag{6}$$

Provided $p \leqslant p_{\rm th}$, such k can be found. Then, we have the threshold theorem of quantum computation [24]. Different FTQC structures result in different thresholds, but the maximum threshold has been 10^{-2} [25], until now.

From FTQC theory, one error-correction period comprises a fault-tolerant encoding circuit, a decoding circuit, and a few steps of fault-tolerant computation between them [31]. The parameter permitted depth of logical operation discussed herein just limits the number of operations on any physical qubit in one error-correction period.

2.3 Description of dynamics of an open quantum system

Assume that the initial state we are interested in is ρ and the environment starts with the state $\rho_{\rm env}$. After the transformation U on the whole system, the reduced state of the system alone is [24]

$$\mathcal{E}(\rho) = {\rm tr}_{\rm env}[U(\rho \otimes \rho_{\rm env})U^\dagger]. \tag{7}$$

$\mathcal{E}$ is a hyperoperator, which has operator-sum representation and natural (linear) representation. The operator-sum representation is expressed as [24]

$$\mathcal{E}(\rho) = \textstyle\sum_k \langle e_k|U(\rho \otimes |e_0\rangle\langle e_0|)U^\dagger|e_k\rangle = \displaystyle\sum_k E_k \rho E_k^\dagger, \tag{8}$$

with $E_k \equiv \langle e_k|U|e_0\rangle$ an operator on the state space of the principal system. The natural (linear) representation [32] is a linear map $N_{\mathcal{E}}$ satisfying $N_{\mathcal{E}}\vec{\rho} = \overrightarrow{(\mathcal{E}(\rho))}$. The two representations are equivalent, and we have found the following relation: Given the operator-sum representation in (8), if we let

$$N_{\mathcal{E}} = E_1 \otimes (E_1^\dagger)^{\rm T} + E_2 \otimes (E_2^\dagger)^{\rm T} + \cdots = E_1 \otimes E_1^* + E_2 \otimes E_2^* + \cdots,$$

we can get $N_{\mathcal{E}}\vec{\rho} = \overrightarrow{(\mathcal{E}(\rho))}$, which is just the natural representation.

3 Qubit states after one Cirac-Zoller CNOT gate driven by a quantized field

3.1 Description of ion-trap QCs driven by a quantized field

Physically, the ions in the ion-trap QC act as an open system, with different laser pulses in the environment. For the purpose of identifying the error from the quantum nature of the driving laser field, the

most straightforward method is to find the dynamics of the qubits in the most natural way (which is also the most complicated way, as in (7)). For each step of the CNOT gates, from the initial state of the ions and the driving laser fields, we apply the transformation on the system of qubits and laser field and then perform a partial trace over the laser fields to obtain the state of the qubits. We provide a description of the whole system at first.

A Cirac-Zoller QC system comprises cold ions confined in a linear trap that interact with the laser beams. According to [22], for estimating the upper bound of the CNOT operation number, it is reasonable to use the Jaynes-Cummings model for the free-space case. We extend the model in [33] to N-ions case and obtain the Hamiltonian for each step of the Cirac-Zoller scheme in the interaction picture as

$$\begin{aligned} H \;=\; & \frac{1}{2}\Omega \sin\theta (a^\dagger \sigma_- \mathrm{e}^{\mathrm{i}(\omega-\omega_0)t}\mathrm{e}^{-\mathrm{i}\phi} + a^\dagger \sigma_+ \mathrm{e}^{\mathrm{i}(\omega+\omega_0)t}\mathrm{e}^{\mathrm{i}\phi} + \text{h.c.}) \\ & + \frac{\eta\Omega}{2\sqrt{N}} \cos\theta (a^\dagger b^\dagger \sigma_- \mathrm{e}^{\mathrm{i}(\omega-\omega_0+\omega_\mathrm{t})t}\mathrm{e}^{-\mathrm{i}\phi} + a^\dagger b \sigma_- \mathrm{e}^{\mathrm{i}(\omega-\omega_0-\omega_\mathrm{t})t}\mathrm{e}^{-\mathrm{i}\phi} \\ & + a^\dagger b^\dagger \sigma_+ \mathrm{e}^{\mathrm{i}(\omega+\omega_0+\omega_\mathrm{t})t}\mathrm{e}^{\mathrm{i}\phi} + a^\dagger b \sigma_+ \mathrm{e}^{\mathrm{i}(\omega+\omega_0-\omega_\mathrm{t})t}\mathrm{e}^{\mathrm{i}\phi} + \text{h.c.}), \end{aligned}$$

where Ω is the coupling parameter between the ion and radiation field; θ accounts for the relative position of the center of mass (CM) of the ion with respect to the standing wave; $a^\dagger$ and a are the creation and destruction operators, respectively, of the radiation field; $b^\dagger$ and b are the creation and destruction operators, respectively, of the CM vibrational phonons; σ_+ and σ_- are the raising and lowering operators, respectively, of the two-level ion; ω is the frequency of radiation field; ω_0 is the frequency difference between the ion's two levels $|0\rangle$ and $|1\rangle$; ω_t is the trap (phonon) frequency; ϕ is the laser phase; and η is the Lamb-Dick parameter. The rotating-wave approximation can be taken to drop the energy non-conserving terms. Considering the operations needed to implement the CNOT gate in Subsection 2.1, we have the corresponding unitary evolution for the quantized driving field case.

- Carrier excitation, where

$$H_1 = \hbar g (a^\dagger \sigma_- \mathrm{e}^{-\mathrm{i}\phi} + a \sigma_+ \mathrm{e}^{\mathrm{i}\phi}), \tag{9}$$

where $g = \frac{1}{2}\Omega \sin\theta$. The corresponding unitary operator is

$$\begin{aligned} U_1(t,\phi) = & \cos\left(gt\sqrt{a^\dagger a + 1}\right)|1\rangle\langle 1| + \cos\left(gt\sqrt{a^\dagger a}\right)|0\rangle\langle 0| \\ & -\mathrm{i}\left[\mathrm{e}^{\mathrm{i}\phi}\frac{\sin(gt\sqrt{a^\dagger a+1})}{\sqrt{a^\dagger a+1}} a|1\rangle\langle 0| + \mathrm{e}^{-\mathrm{i}\phi} a^\dagger \frac{\sin(gt\sqrt{a^\dagger a+1})}{\sqrt{a^\dagger a+1}}|0\rangle\langle 1|\right]. \end{aligned} \tag{10}$$

- Red sideband excitation, where

$$H_2 = g'(a^\dagger b^\dagger \sigma_- \mathrm{e}^{-\mathrm{i}\phi} + ab\sigma_+ \mathrm{e}^{\mathrm{i}\phi}),$$

where $g' = \frac{\eta\Omega}{2\sqrt{N}}\cos\theta$. The unitary operator is

$$\begin{aligned} U_2(t,\phi) = & \cos\left(g't\sqrt{(a^\dagger a+1)(b^\dagger b+1)}\right)|1\rangle\langle 1| + \cos\left(g't\sqrt{a^\dagger a b^\dagger b}\right)|0\rangle\langle 0| \\ & -\mathrm{i}\left[\mathrm{e}^{\mathrm{i}\phi}\frac{\sin(g't\sqrt{(a^\dagger a+1)(b^\dagger b+1)})}{\sqrt{(a^\dagger a+1)(b^\dagger b+1)}} ab|1\rangle\langle 0| + \mathrm{e}^{-\mathrm{i}\phi} a^\dagger b^\dagger \frac{\sin(g't\sqrt{(a^\dagger a+1)(b^\dagger b+1)})}{\sqrt{(a^\dagger a+1)(b^\dagger b+1)}}|0\rangle\langle 1|\right]. \end{aligned} \tag{11}$$

3.2 State after one CNOT gate driven by a quantized field

From the above-mentioned discussion, for the implementation of a CNOT gate, the system comprises a two-level ion, a motional degree of freedom (phonon), and a laser field (in free space). For the xth ion, the two-level system we choose as the qubit has levels $|0\rangle_x$ and $|1\rangle_x$; for the yth ion, in addition to the two-level system containing $|0\rangle_y$ and $|1\rangle_y$, an auxiliary level $|\mathrm{aux}\rangle_y$ is used to complete the CNOT

operation [8]. For the phonon, the two levels used as qubit are denoted as $|0\rangle_{\rm ph}$ and $|1\rangle_{\rm ph}$. For the system comprising the xth ion, yth ion, and phonon, the initial state is generally a superposition of the computational basis:

$$\begin{aligned}|\psi(0)\rangle =& \alpha_1|0\rangle_x|0\rangle_y|0\rangle_{\rm ph}+\alpha_2|1\rangle_x|0\rangle_y|0\rangle_{\rm ph}+\alpha_3|0\rangle_x|1\rangle_y|0\rangle_{\rm ph}+\alpha_4|1\rangle_x|1\rangle_y|0\rangle_{\rm ph}\\ &+\alpha_5|0\rangle_x|{\rm aux}\rangle_y|0\rangle_{\rm ph}+\alpha_6|1\rangle_x|{\rm aux}\rangle_y|0\rangle_{\rm ph}+\alpha_7|0\rangle_x|0\rangle_y|1\rangle_{\rm ph}+\alpha_8|1\rangle_x|0\rangle_y|1\rangle_{\rm ph}\\ &+\alpha_9|0\rangle_x|1\rangle_y|1\rangle_{\rm ph}+\alpha_{10}|1\rangle_x|1\rangle_y|1\rangle_{\rm ph}+\alpha_{11}|0\rangle_x|{\rm aux}\rangle_y|1\rangle_{\rm ph}+\alpha_{12}|1\rangle_x|{\rm aux}\rangle_y|1\rangle_{\rm ph}.\end{aligned}\tag{12}$$

Generally, the phonons are cooled to $|0\rangle$, initially in the experiment, and the states of the ions are relatively simple. Then, the coefficients of some computational basis in the above equation may be zero. However, for achieving the quantum transformation of the qubits after one CNOT gate, it is necessary to let the initial state be a general state so as to obtain the right transformation. Then the initial state for qubits (xth ion, yth ion, and phonon) is $\rho^{(0)}=|\psi(0)\rangle\ \langle\psi(0)|$.

The single-mode quantized coherent field can be written as $|\psi^{(n)}\rangle_{\rm l}=\sum_{n=0}^{\infty}c_n|n\rangle_{\rm l}$, with $|c_n|^2=\frac{{\rm e}^{-\bar{n}}\bar{n}^n}{n!}$. This expression is summed over n, and it seems unnecessary to label the state with n. However, because the laser fields are different in each step of one CNOT gate, the parameter n can be seen as a way to distinguish the fields. Then, we can let the initial state for the environment (laser field) be $\rho_{lm}=|\psi^{(m)}\rangle_{\rm l}\langle\psi^{(m)}|$, $\rho_{ln}=|\psi^{(n)}\rangle_{\rm l}\langle\psi^{(n)}|$, $\rho_{lp}=|\psi^{(p)}\rangle_{\rm l}\langle\psi^{(p)}|$, $\rho_{lq}=|\psi^{(q)}\rangle_{\rm l}\langle\psi^{(q)}|$, $\rho_{lr}=|\psi^{(r)}\rangle_{\rm l}\langle\psi^{(r)}|$ for each step of CNOT gate.

Step 1. The interaction is carrier excitation, and the unitary evolution operator $U_1(t,\phi)$ in (10) can be applied. The laser field and the yth ion are evolved. The duration t_1 of the $\pi/2$ pulse satisfies $gt_1\sqrt{\bar{m}}=\pi/4$ [21], and $\phi=-\pi/2$. The aim is to compute

$$\begin{aligned}\rho_{\rm step1}^{(1)}=&{\rm tr}_{lm}\Big[U_1(t_1,-\pi/2)(\rho^{(0)}\otimes\rho_{lm})U_1(t_1,-\pi/2)^\dagger\Big]\\ =&{\rm tr}_{lm}\Big[\Big(U_1(t_1,-\pi/2)(|\psi(0)\rangle\otimes|\psi^{(m)}\rangle_{\rm l})\Big)\Big(U_1(t_1,-\pi/2)(|\psi(0)\rangle\otimes|\psi^{(m)}\rangle_{\rm l})\Big)^\dagger\Big],\end{aligned}\tag{13}$$

where $U_1(t_1,-\pi/2)(|\psi(0)\rangle\otimes|\psi^{(m)}\rangle_{\rm l})$ can be obtained with

$$U_1(t_1,-\pi/2)\Big(|0\rangle_y\otimes|\psi^{(m)}\rangle_{\rm l}\Big)=\sum_{m=0}^{\infty}c_m\cos\frac{\pi\sqrt{m}}{4\sqrt{\bar{m}}}|0\rangle_y|m\rangle-\sum_{m=0}^{\infty}c_m\sin\frac{\pi\sqrt{m}}{4\sqrt{\bar{m}}}|1\rangle_y|m-1\rangle$$

and

$$U_1(t_1,-\pi/2)\Big(|1\rangle_y\otimes|\psi^{(m)}\rangle_{\rm l}\Big)=\sum_{m=0}^{\infty}c_m\cos\frac{\pi\sqrt{m+1}}{4\sqrt{\bar{m}}}|1\rangle_y|m\rangle+\sum_{m=0}^{\infty}c_m\sin\frac{\pi\sqrt{m+1}}{4\sqrt{\bar{m}}}|0\rangle_y|m+1\rangle.$$

We can see the operation on an ion with state $|0\rangle_y$ gives a mixed state of the ion and laser field (labeled m), different from $\frac{1}{\sqrt{2}}(|0\rangle_y-|1\rangle_y)$ driven by a classical field in (2) (the case for $|1\rangle_y$ is similar). Once $U_1(t_1,-\pi/2)(|\psi(0)\rangle\otimes|\psi^{(m)}\rangle_{\rm l})$ is obtained, we trace out the laser field and obtain the state of the qubits (xth ion, yth ion and phonon) $\rho_{\rm step1}^{(1)}$ from (13).

Step 2. The interaction is the red sideband excitation, and the unitary evolution operator $U_2(t,\phi)$ in (11) can be applied. The second laser field, xth ion, and phonons are evolved. The duration t_2 of the π pulse satisfies $gt_2\sqrt{\bar{n}}=\pi/2$, and $\phi=0$. The aim is to compute

$$\rho_{\rm step2}^{(1)}={\rm tr}_{ln}\Big[U_2(t_2,0)(\rho_{\rm step1}^{(0)}\otimes\rho_{ln})U_2(t_2,0)^\dagger\Big],\tag{14}$$

which can be obtained with

$$U_2(t_2,0)\Big(|\psi^{(n)}\rangle_{\rm l}|1\rangle_x|0\rangle_{\rm ph}\Big)=\sum_{n=0}^{\infty}c_n\cos\frac{\pi\sqrt{n+1}}{2\sqrt{\bar{n}}}|n\rangle|1\rangle_x|0\rangle_{\rm ph}-{\rm i}\sum_{n=0}^{\infty}c_n\sin\frac{\pi\sqrt{n+1}}{2\sqrt{\bar{n}}}|n+1\rangle|0\rangle_x|1\rangle_{\rm ph},$$

and

$$U_2(t_2,0)\Big(|\psi^{(n)}\rangle_{\rm l}|0\rangle_x|1\rangle_{\rm ph}\Big)=\sum_{n=0}^{\infty}c_n\cos\frac{\pi\sqrt{n}}{2\sqrt{\bar{n}}}|n\rangle|0\rangle_x|1\rangle_{\rm ph}-{\rm i}\sum_{n=0}^{\infty}c_n\sin\frac{\pi\sqrt{n}}{2\sqrt{\bar{n}}}|n-1\rangle|1\rangle_x|0\rangle_{\rm ph}.$$

The operation on $|1\rangle_x|0\rangle_{\rm ph}$ of an ion and phonon gives a mixed state with laser field (labeled n), and there is still population left on $|1\rangle_x|0\rangle_{\rm ph}$, different from $-{\rm i}|0\rangle_x|1\rangle_{\rm ph}$ driven by the classical field in (4) (The case for $|0\rangle_x|1\rangle_{\rm ph}$ is similar). We then trace out the laser field and obtain the state of the qubits $\rho^{(1)}_{step2}$ from (14).

Step 3. The interaction is the red sideband excitation, and the unitary evolution operator is $U_2(t,\phi)$ in (11). The third laser field, yth ion, and phonons are evolved. The duration t_3 of the 2π pulse satisfies $gt_3\sqrt{\bar{p}}=\pi$, and $\phi=0$. From $U_2(t_3,0)(|\psi^{(p)}\rangle_{\rm l}|0\rangle_y|1\rangle_{\rm ph})=\sum_{p=0}^{\infty}c_p\cos\frac{\pi\sqrt{p+1}}{\sqrt{\bar{p}}}|p\rangle|0\rangle_y|1\rangle_{\rm ph}-{\rm i}\sum_{p=0}^{\infty}c_p\sin\frac{\pi\sqrt{p+1}}{\sqrt{\bar{p}}}|p+1\rangle|{\rm aux}\rangle_y|0\rangle_{\rm ph}$ and $U_2(t_3,0)(|\psi^{(p)}\rangle_{\rm l}|{\rm aux}\rangle_y|0\rangle_{\rm ph})=\sum_{p=0}^{\infty}c_p\cos\frac{\pi\sqrt{p}}{\sqrt{\bar{p}}}|p\rangle|{\rm aux}\rangle_y|0\rangle_{\rm ph}-{\rm i}\sum_{p=0}^{\infty}c_p\sin\frac{\pi\sqrt{p}}{\sqrt{\bar{n}}}|p-1\rangle|0\rangle_y|1\rangle_{\rm ph}$, we can get the state of the qubits $\rho^{(1)}_{\rm step3}={\rm tr}_{lp}[U_2(t_3,0)(\rho^{(0)}_{\rm step2}\otimes\rho_{lp})U_2(t_3,0)^\dagger]$.

Step 4. This step is the same as Step 2. State of the qubits $\rho^{(1)}_{\rm step4}={\rm tr}_{lq}[U_2(t_2,0)(\rho^{(0)}_{\rm step3}\otimes\rho_{lp})U_2(t_2,0)^\dagger]$ can be obtained.

Step 5. This step is similar to Step 1. State of the qubits $\rho^{(1)}_{\rm step5}={\rm tr}_{lr}[U_1(t_1,\pi/2)(\rho^{(0)}_{\rm step4}\otimes\rho_{lr})U_1(t_1,\pi/2)^\dagger]$ can be obtained.

Then, the density matrix after one CNOT gate for the qubits (xth ion, yth ion, and phonon) is $\rho^{(1)}=\rho^{(1)}_{\rm step5}$. It has 144 elements, with

$$\begin{aligned}
\rho^{(1)}_{1,1}&=\Big[(S_1^2+2S_2S_4+S_5S_{10})\alpha_1+(S_4(S_1-S_3+S_7)-S_6S_{10})\alpha_3\Big]\alpha_1^*\\
&\quad+\alpha_3^*\Big[\alpha_1S_1S_4-\alpha_1S_3S_4-\alpha_1S_6S_{10}+\alpha_1S_4S_7+\alpha_3S_1S_{10}\\
&\quad-2\alpha_3S_4S_9+\alpha_3S_8S_{10}\Big],\\
&\vdots\\
\rho^{(1)}_{12,11}&=-\alpha_{12}\Big[-S_{26}^2\alpha_{11}^*+S_{23}\Big(S_{13}S_{37}\alpha_{10}^*+S_{28}S_{40}\alpha_{11}^*-{\rm i}(S_{26}+S_{19}S_{40})\alpha_6^*+S_3S_{37}\alpha_8^*\Big)\Big],\\
\rho^{(1)}_{12,12}&=\alpha_{12}\alpha_{12}^*.
\end{aligned}$$

where

$$\begin{aligned}
S_1&=\sum_{n=0}^{\infty}\frac{{\rm e}^{-\bar{n}}\bar{n}^n}{n!}\cos^2\left(\frac{\pi\sqrt{n}}{4\sqrt{\bar{n}}}\right), & S_2&=\sum_{n=0}^{\infty}\frac{{\rm e}^{-\bar{n}}\bar{n}^n}{n!}\sqrt{\frac{\bar{n}}{n+1}}\cos\left(\frac{\pi\sqrt{n}}{4\sqrt{\bar{n}}}\right)\sin\left(\frac{\pi\sqrt{n+1}}{4\sqrt{\bar{n}}}\right),\\
S_3&=\sum_{n=0}^{\infty}\frac{{\rm e}^{-\bar{n}}\bar{n}^n}{n!}\cos\left(\frac{\pi\sqrt{n}}{4\sqrt{\bar{n}}}\right)\cos\left(\frac{\pi\sqrt{n+1}}{4\sqrt{\bar{n}}}\right), & S_4&=\frac{1}{2}\sum_{n=0}^{\infty}\frac{{\rm e}^{-\bar{n}}\bar{n}^n}{n!}\sqrt{\frac{n}{\bar{n}}}\sin\left(\frac{\pi\sqrt{n}}{2\sqrt{\bar{n}}}\right),\\
S_5&=\sum_{n=0}^{\infty}\frac{{\rm e}^{-\bar{n}}\bar{n}^n}{n!}\sin^2\left(\frac{\pi\sqrt{n}}{4\sqrt{\bar{n}}}\right), & S_6&=\frac{1}{2}\sum_{n=0}^{\infty}\frac{{\rm e}^{-\bar{n}}\bar{n}^n}{n!}\sqrt{\frac{\bar{n}}{n+1}}\sin\left(\frac{\pi\sqrt{n+1}}{2\sqrt{\bar{n}}}\right),\\
S_7&=\sum_{n=0}^{\infty}\frac{{\rm e}^{-\bar{n}}\bar{n}^n}{n!}\sqrt{\frac{n}{n+1}}\sin\left(\frac{\pi\sqrt{n}}{4\sqrt{\bar{n}}}\right)\sin\left(\frac{\pi\sqrt{n+1}}{4\sqrt{\bar{n}}}\right), & S_8&=\sum_{n=0}^{\infty}\frac{{\rm e}^{-\bar{n}}\bar{n}^n}{n!}\cos^2\left(\frac{\pi\sqrt{n+1}}{4\sqrt{\bar{n}}}\right),\\
S_9&=\sum_{n=0}^{\infty}\frac{{\rm e}^{-\bar{n}}\bar{n}^n}{n!}\sqrt{\frac{n}{\bar{n}}}\cos\left(\frac{\pi\sqrt{n+1}}{4\sqrt{\bar{n}}}\right)\sin\left(\frac{\pi\sqrt{n}}{4\sqrt{\bar{n}}}\right), & S_{10}&=\sum_{n=0}^{\infty}\frac{{\rm e}^{-\bar{n}}\bar{n}^n}{n!}\sin^2\left(\frac{\pi\sqrt{n+1}}{4\sqrt{\bar{n}}}\right),\\
S_{13}&=\sum_{n=0}^{\infty}\frac{{\rm e}^{-\bar{n}}\bar{n}^n}{n!}\sqrt{\frac{n}{\bar{n}}}\sin\left(\frac{\pi\sqrt{n}}{4\sqrt{\bar{n}}}\right), & S_{19}&=\sum_{n=0}^{\infty}\frac{{\rm e}^{-\bar{n}}\bar{n}^n}{n!}\cos\left(\frac{\pi\sqrt{n+1}}{2\sqrt{\bar{n}}}\right),\\
S_{23}&=\sum_{n=0}^{\infty}\frac{{\rm e}^{-\bar{n}}\bar{n}^n}{n!}\sqrt{\frac{n}{\bar{n}}}\sin\left(\frac{\pi\sqrt{n}}{2\sqrt{\bar{n}}}\right), & S_{26}&=\sum_{n=0}^{\infty}\frac{{\rm e}^{-\bar{n}}\bar{n}^n}{n!}\cos\left(\frac{\pi\sqrt{n}}{2\sqrt{\bar{n}}}\right),\\
S_{28}&=\sum_{n=0}^{\infty}\frac{{\rm e}^{-\bar{n}}\bar{n}^n}{n!}\sqrt{\frac{\bar{n}}{n+1}}\sin\left(\frac{\pi\sqrt{n+1}}{2\sqrt{\bar{n}}}\right), & S_{37}&=\sum_{n=0}^{\infty}\frac{{\rm e}^{-\bar{n}}\bar{n}^n}{n!}\sqrt{\frac{n}{\bar{n}}}\sin\left(\frac{\pi\sqrt{n}}{\sqrt{\bar{n}}}\right),\\
S_{40}&=\sum_{n=0}^{\infty}\frac{{\rm e}^{-\bar{n}}\bar{n}^n}{n!}\cos\left(\frac{\pi\sqrt{n}}{\sqrt{\bar{n}}}\right).
\end{aligned}\tag{15}$$

There are 42 sums such as S_i ($i=1,2,\ldots$) above in $\rho^{(1)}$ and obtaining a high-precision result for the sums above is difficult. The usual algorithm (saddle-point approximation [34, 35]) using the numerical

Table 1 Values of S_i $(i = 1, 2, \ldots, 42)$

Sum	Value	Sum	Value
S_1	0.50000009817476291019827255429 9	S_{22}	0.99999888315017320180806477611 8
S_2	0.49999997963696941606489820113 7	S_{23}	0.99999956657491317120098244485 6
S_3	0.49999990182521952313653007084 2	S_{24}	$6.16850164435813122850485011055 0 \times 10^{-7}$
S_4	0.49999978328745658560049122242 8	S_{25}	$5.89048329267195769677246638410 8 \times 10^{-7}$
S_5	0.49999990182523708980172744570 1	S_{26}	$1.96349525820396545108597414916 7 \times 10^{-7}$
S_6	0.49999978328745658560049122242 8	S_{27}	0.99999938314983556418687714951 5
S_7	0.49999984817478813273492221602 7	S_{28}	0.99999956657491317120098244485 6
S_8	0.49999970547575324235230488982 7	S_{29}	0.99999753260514199680208496959 6
S_9	0.49999958693796482361878398902 3	S_{30}	$3.92694731763846972895928960781 0 \times 10^{-7}$
S_{10}	0.50000029452424675764769511017 3	S_{31}	0.99999753260452514774675027703 3
S_{11}	0.70710679608421657198284726413 5	S_{32}	$3.92698607538142196426437000386 3 \times 10^{-7}$
S_{12}	0.70710651840404689913721178460 7	S_{33}	$-0.99999876630028797819009097432$
S_{13}	$0.70710670769587146721002744979 8 \times 10^{-7}$	S_{34}	$2.46739485800319791503040372042 1 \times 10^{-6}$
S_{14}	0.70710670769587146721002744979 8	S_{35}	$3.92698607538142196426437000382 5 \times 10^{-7}$
S_{15}	$6.16849856010904954512839682968 2 \times 10^{-7}$	S_{36}	$2.46739300745180671853161538037 \times 10^{-6}$
S_{16}	$-1.96349546006718133137558424000 \times 10^{-7}$	S_{37}	$-3.92699092013436266275116848001 \times 10^{-7}$
S_{17}	$6.16849701798257544217879612403 9 \times 10^{-7}$	S_{38}	0.99999753260390830477948054801 5
S_{18}	$-1.96349546006718133137558424000 \times 10^{-7}$	S_{39}	$3.92702483317282139941109276693 0 \times 10^{-7}$
S_{19}	$-5.89048493515295390220345714779 \times 10^{-7}$	S_{40}	$-0.99999876629967112837375429903 0$
S_{20}	0.99999938315014398909504548716 0	S_{41}	$2.46739609169522051945198452981 1 \times 10^{-6}$
S_{21}	0.49995869453343231184832164785 6	S_{42}	$-3.92699092013436266275116848001 \times 10^{-7}$

method can reach a precision of $1/\sqrt{\bar{n}}$ only, which cannot satisfy the need for iteration in the full quantum theory of the interaction. Our former study [22] presented an algorithm using both numerical and analytic methods and could achieve any given precision. The values of S_i $(i = 1, \ldots, 42)$ when $\bar{n} = 10^6$ are shown in Table 1.

3.3 Quantum transformation after N CNOT operations

Consider the state transformation for the qubits after one CNOT operation with initial state $\rho^{(0)} = |\psi^{(0)}\rangle\langle\psi^{(0)}|$. From the definition of natural (linear) representation of operators, we can get $\overrightarrow{\rho^{(1)}_{\text{step1}}} = M_1\overrightarrow{\rho^{(0)}}$, with M_1 a matrix of a linear map. Here, $\vec{\rho}$ is the realignment of matrix ρ. Similarly, if we let the corresponding matrices of Steps 2–5 be M_2, M_3, M_4, M_5, then

$$\overrightarrow{\rho^{(1)}} = M\overrightarrow{\rho^{(0)}}, \tag{16}$$

where $M = M_5M_4M_3M_2M_1$.

According to the previous calculation, $\rho^{(0)}$ and $\rho^{(1)}$ are both 12×12 matrices. Then, $\overrightarrow{\rho^{(0)}}$ and $\overrightarrow{\rho^{(1)}}$ are 144×1 column vectors. From (16), we can see that the matrix M, corresponding to one CNOT operation is of the size 144×144. Therefore, we need to determine the 144×144 elements.

We can only obtain 144 equations from the rule of matrix multiplication from (16). Then, we examine each equation, because $\alpha_1, \ldots, \alpha_{12}$ defined in $\rho^{(0)}$ is any set of complex numbers with modular square sum 1, then the coefficients of $\alpha_1\alpha_1^*, \alpha_1\alpha_2^*, \ldots, \alpha_{12}\alpha_{12}^*$ should be the same on both sides of each equation. Finally, we have 144×144 equations in all, which is sufficient to determine M. Lengthy computations finally provide the elements of M as follows, and we find that M is independent of the initial state.

$$\begin{aligned}
&M_{1,1} = S_1^2 + 2S_2S_4 + S_5S_{10},\\
&M_{1,2} = 0,\\
&M_{1,3} = S_1S_4 - S_3S_4 - S_{10}S_6 + S_4S_8,\\
&\vdots
\end{aligned}$$

$$M_{144,142} = 0,$$
$$M_{144,143} = 0,$$
$$M_{144,144} = 1.$$

4 Permitted depth of logical operation of CNOT gates in ion-trap QC

4.1 Final state and failure probability

Once M is obtained, we can get the state after n times of CNOT operation $\rho^{(N)}$ from $\overrightarrow{\rho^{(N)}} = M\overrightarrow{\rho^{(N-1)}} = \cdots = M^N\overrightarrow{\rho^{(0)}}$.

In the Cirac-Zoller CNOT scheme, the phonons are cooled to state $|0\rangle_{\rm ph}$ in the beginning. The ions are generally in the state $\{|0\rangle_x|0\rangle_y, |0\rangle_x|1\rangle_y, |1\rangle_x|0\rangle_y, |1\rangle_x|1\rangle_y\}$. Thus, the actual initial state of the CNOT operation is $|\widetilde{\psi^{(0)}}\rangle = \alpha_1|0\rangle_x|0\rangle_y|0\rangle_{\rm ph} + \alpha_2|1\rangle_x|0\rangle_y|0\rangle_{\rm ph} + \alpha_3|0\rangle_x|1\rangle_y|0\rangle_{\rm ph} + \alpha_4|1\rangle_x|1\rangle_y|0\rangle_{\rm ph}$. For the final state $\rho^{(N)}$, we are interested in the state of ions. We can trace the freedom of phonons out to get the final state $\rho^{(N)'}$. The actual final state is $\widetilde{\rho^{(N)}} = \rho^{(N)'}|_{\alpha_5,\ldots,\alpha_{12}=0}$.

To obtain the failure probability of the CNOT operation, we first need to know the expected state. It can be written as $|\psi_e\rangle = \alpha_1|0\rangle_x|0\rangle_y + \alpha_2|1\rangle_x|0\rangle_y + \alpha_3|0\rangle_x|1\rangle_y + \alpha_4|1\rangle_x|1\rangle_y$ when the number of CNOT operations is even. When the operation number is odd, the expected state is $|\psi_e\rangle = \alpha_1|0\rangle_x|0\rangle_y + \alpha_4|1\rangle_x|0\rangle_y + \alpha_3|0\rangle_x|1\rangle_y + \alpha_2|1\rangle_x|1\rangle_y$. The failure probability is

$$\begin{aligned} p_f = 1 - p_s = 1 - \langle\psi_e|\widetilde{\rho^{(N)}}|\psi_e\rangle = {} & |\alpha_1|^2\widetilde{\rho^{(N)}}_{11} - \alpha_1^*\alpha_2\widetilde{\rho^{(N)}}_{12} - \alpha_1{}^*\alpha_3\widetilde{\rho^{(N)}}_{13} - \alpha_1{}^*\alpha_4\widetilde{\rho^{(N)}}_{14} \\ & -\alpha_1\alpha_2{}^*\widetilde{\rho^{(N)}}_{21} - |\alpha_2|^2\widetilde{\rho^{(N)}}_{22} + \alpha_2{}^*\alpha_3\widetilde{\rho^{(N)}}_{23} + \alpha_2{}^*\alpha_4\widetilde{\rho^{(N)}}_{24} + \alpha_1\alpha_3{}^*\widetilde{\rho^{(N)}}_{31} + \alpha_2\alpha_3{}^*\widetilde{\rho^{(N)}}_{32} \\ & +|\alpha_3|^2\widetilde{\rho^{(N)}}_{33} + \alpha_3{}^*\alpha_4\widetilde{\rho^{(N)}}_{34} + \alpha_1\alpha_4{}^*\widetilde{\rho^{(N)}}_{41} + \alpha_2\alpha_4{}^*\widetilde{\rho^{(N)}}_{42} + \alpha_3\alpha_4{}^*\widetilde{\rho^{(N)}}_{43} + |\alpha_4|^2\widetilde{\rho^{(N)}}_{44}, \end{aligned}$$

where $\widetilde{\rho^{(N)}}_{ij}$ $(i,j \in 1,2,3,4)$ are elements of the ions' density matrix after N CNOT gates and are functions of S_i (with the form $\sum_{n=0}^{\infty}\frac{{\rm e}^{-\bar{n}}\bar{n}^n}{n!}f_{i0}(n,\bar{n},k)$, and $i = 1,2,\ldots,42$) in Section 3 of the paper. The logarithm of failure probability to operation number is plotted in Figure 1, for different initial states and mean numbers of photons. The first four curves from the bottom to the top represent the cases of $\bar{n} = 10^6$, with the initial state being $|0\rangle_x|0\rangle_y$, $|0\rangle_x|1\rangle_y$, $|1\rangle_x|0\rangle_y$, and $|1\rangle_x|1\rangle_y$, respectively. The 5th to 8th curves from the bottom to the top represent the cases of $\bar{n} = 10^4$, with the initial state being $|0\rangle_x|0\rangle_y$, $|0\rangle_x|1\rangle_y$, $|1\rangle_x|0\rangle_y$, and $|1\rangle_x|1\rangle_y$, successively. At first, we may see only six lines instead of eight. This is because the failure probabilities under the initial states $|1\rangle_x|0\rangle_y$ and $|1\rangle_x|1\rangle_y$ are almost the same, and the corresponding curves overlap in Figure 1. A possible physical reason may be that for the initial state $|1\rangle_x|0\rangle_y$, the result after one CNOT gate is nearly $|1\rangle_x|1\rangle_y$, with a small error of the order 10^{-4} from quantum nature of driving field. Then, the evolution after N CNOT gates on initial state $|1\rangle_x|0\rangle_y$ is almost the same with that after $(N-1)$ CNOT gates on $|1\rangle_x|1\rangle_y$. Thus, the failure probability after N CNOT gates on the initial state $|1\rangle_x|0\rangle_y$ and $|1\rangle_x|1\rangle_y$ are almost the same.

As seen in Figure 1, as the operation number increases and the mean number of photons decreases, the failure probability after many CNOT operations increases. Indeed, the failure probability has a complicated theoretical relation with the mean number of photons. Moreover, the failure probability is different for different initial states. If the initial state is $|1\rangle_x|0\rangle_y$ or $|1\rangle_x|1\rangle_y$, the failure probability is relatively large; if the initial state is $|0\rangle_x|0\rangle_y$ or $|0\rangle_x|1\rangle_y$, the failure probability is relatively small. If the initial state is a superposition of the four states mentioned above, a more general rule works: if the amplitude of $|1\rangle_x|0\rangle_y$ or $|1\rangle_x|1\rangle_y$ is large, the failure probability is large; however, if the amplitude of $|0\rangle_x|0\rangle_y$ or $|0\rangle_x|1\rangle_y$ is large, the failure probability is small. This can be interpreted as follows. From the Cirac-Zoller CNOT gate scheme [8], for the 5 steps in Cirac-Zoller CNOT gate, the quantized fields in Steps 1 and 5 act on all states of the yth qubit, thus affect all the initial state $|0\rangle_x|0\rangle_y$, $|0\rangle_x|1\rangle_y$, $|1\rangle_x|0\rangle_y$, and $|1\rangle_x|1\rangle_y$; Steps 2–4 act only on certain state of qubits, for example, the quantized field in Step 2 acts only on $|1\rangle_x|0\rangle_{\rm ph}$, $|0\rangle_x|1\rangle_{\rm ph}$. The input for Step 2 (i.e., output from Step 1 which keeps xth ion and

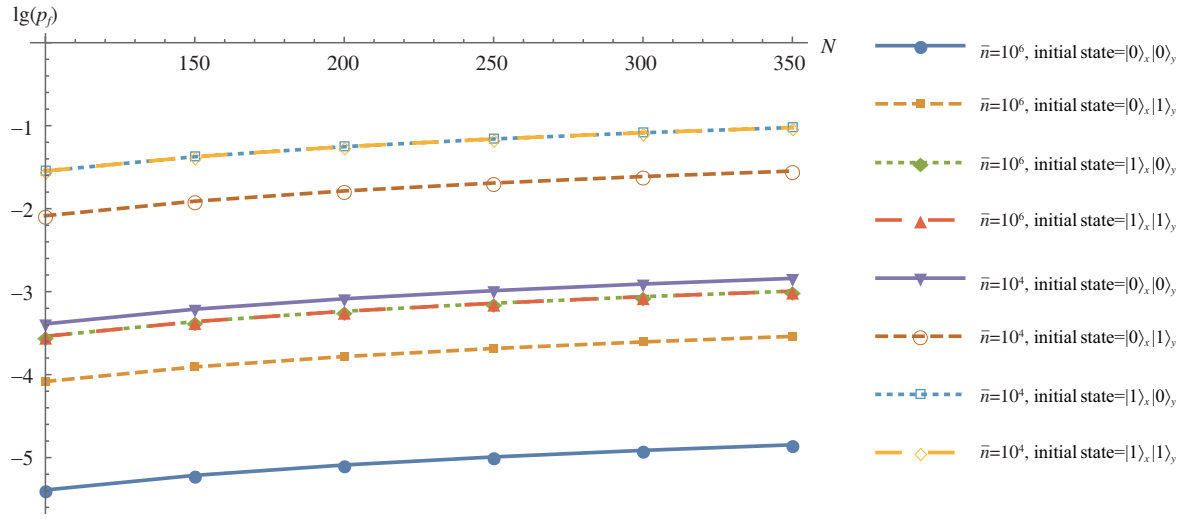

Figure 1 (Color online) Failure probability from field quantization for different initial states and $\bar{n}$. Here, N denotes the operation number and p_f denotes the failure probability. The failure probabilities under the initial state $|1\rangle_x|0\rangle_y$ and $|1\rangle_x|1\rangle_y$ are almost the same, and the corresponding curves overlap in both the cases of $\bar{n} = 10^6$ and $\bar{n} = 10^4$.

phonon unchanged) under initial state $|0\rangle_x|0\rangle_y$, $|0\rangle_x|1\rangle_y$, $|1\rangle_x|0\rangle_y$, $|1\rangle_x|1\rangle_y$ (with phonons in $|0\rangle_{\rm ph}$) are $|0\rangle_x|0\rangle_{\rm ph}$, $|0\rangle_x|0\rangle_{\rm ph}$, $|1\rangle_x|0\rangle_{\rm ph}$, $|1\rangle_x|0\rangle_{\rm ph}$, respectively, then in Step 2 the ions under initial state $|0\rangle_x|0\rangle_y$, $|0\rangle_x|1\rangle_y$ are not affected, while the ions under initial state $|1\rangle_x|0\rangle_y$, $|1\rangle_x|1\rangle_y$ are driven by the quantized laser field. Thus the evolution under initial states $|1\rangle_x|0\rangle_y$ and $|1\rangle_x|1\rangle_y$ are more affected by the quantized driving field, resulting more error.

4.2 Failure probability when the limitation to $\bar{n}$ is considered

For the failure probability obtained above, we cannot simply decrease the error by increasing the laser intensity. On the one hand, according to the original paper [8], the implementation of the Cirac-Zoller CNOT gate needs sufficiently low laser intensities, to only cause the transition that modifies one of the collective normal modes of ions. On the other hand, our former study [22] showed that, considering the scattering cross-section of laser and an ion [36, 37], and the speed limit for the sideband transitions involved in Steps 2–4 of the Cirac-Zoller CNOT gate [28], the effect mean number of photons was not more than 10^4 when the wavelength was in the typical order of 10^{-6} m.

The driving laser field for the Cirac-Zoller CNOT gate can either be standing or traveling wave. For the traveling wave, to estimate its mean number of photons, we assume a fictitious pulse propagates simultaneously in the opposite direction. They instantly form a standing wave when overlapping in space. The mean number of photons in each pulse is approximately half of those in the standing wave. We now focus on the mean number of photons in the standing wave and obtain the estimation of $\bar{n}$ as in [22].

(1) Relation of mean number of photons $\bar{n}$ and the electric field E for $k\pi$ pulse. The electric field E can be expressed as $E = \mathcal{E}\sqrt{\bar{n}}$, $\mathcal{E}$ is usually given as $\mathcal{E}=\sqrt{\frac{\hbar\omega}{\epsilon_0 V}}$ [38], where ω denotes the frequency of the single mode in a cavity, and V denotes the volume of the cavity.

It can be seen that $V \sim {\rm Act}_0$, with A the cross-sectional area of the beam and t_0 the time duration of the pulse, thus $\bar{n} \sim \frac{\epsilon_0 {\rm Act}_0}{\hbar\omega}E^2$.

For a $k\pi$ pulse, $gt_0\sqrt{\bar{n}} = \frac{k\pi}{2}$ [21], $g \sim \frac{p\mathcal{E}}{\hbar} = \frac{pE}{\hbar\sqrt{\bar{n}}}$, with $p \sim {\rm e}a_0$ the electric dipole moment of the ion, e the charge of an electron, and a_0 the Bohr radius, we thus obtain $t_0 \sim \frac{k\pi\hbar}{2pE}$. Then we have $\bar{n} \sim \frac{k}{4}\frac{\epsilon_0 A\lambda}{p}E$.

(2) Expression of effect mean number of photons considering the scattering cross-section. According to [22], suppose we have a uniform laser beam A, then a photon in the beam has equal probability at any point of the beam's cross-sectional area. However, only the probability amplitude in an "effective interaction area" (around the ion) is useful for the interaction. Thus, in some sense, this

is equivalent to a beam (beam B) with "effective interaction area" interacting with the ion, where any photon's probability amplitude at every point of the beam is useful for the interaction. Then, the mean number of photons in beam B is the effective mean number of photons in beam A. Physically, the "size" of a photon has the order of wavelength λ; then, the effective interaction area of a photon and an ion is of the order λ^2.

A more rigorous result is the following. Consider the resonant scattering cross-section for an atomic dipole transition $\sigma = 3\lambda^2/2\pi$ [36]; because when a photon is scattered in the paraxial mode, there is no interaction, the effective interaction area is estimated to be the cross-section for scattering out of the paraxial modes $\sigma_{\text{eff}} = 3\lambda^2/8\pi$ [37], and the photons in volume $\sigma_{\text{eff}}ct$ is effective. For each photon, the probability of being in area σ_{eff} is $\frac{\sigma_{\text{eff}}}{A}$, and the probabilities are independent of the photons. The effective mean number of photons is

$$\bar{n}_{\text{eff}} = \bar{n}\frac{\sigma_{\text{eff}}}{A} \sim \frac{k}{4}\frac{\epsilon_0\sigma_{\text{eff}}\lambda}{\mathrm{e}a_0}E. \tag{17}$$

For a given $k\pi$ pulse, $\bar{n}_{\text{eff}}$ mainly depends on the value λ and E.

(3) Calculation of $\bar{n}$ when limitation to E in sideband transition is considered. We focus on the sideband transition, which is the main part in implementation of the Cirac-Zoller CNOT gate. The laser detuning $\Delta = \pm\omega_{\text{t}}$, where ω_{t} is the frequency of the trap. Because of the AC-Stark shift and off-resonant transitions, the sideband Rabi frequency Ω_+ has an upper bound. Methods have been adopted to partially cancel the effect, and it seems feasible to have $\Omega_+ < \omega_{\text{t}}$ for special temporal and spectral arrangements of the laser field [28]. As $\Omega_+ = \frac{2\pi}{\lambda}\sqrt{\frac{\hbar}{2m\omega_{\text{t}}}}\Omega$, where m is the mass for a single ion, we have

$$\Omega < \frac{\lambda}{2\pi}\sqrt{\frac{2m}{\hbar}}\omega_{\text{t}}^{\frac{3}{2}}. \tag{18}$$

From [39, 40], it can be seen that

$$\Omega = -\frac{\mathrm{e}a_0E}{4\hbar}, \quad \omega_{\text{t}} = \sqrt{\frac{\mathrm{e}^2}{4\pi\epsilon_0 m z_{\text{s}}^3}}, \tag{19}$$

where z_{s} is the order of the separation between ions and is typically 10 to 100 μm. Suppose $z_{\text{s}} = \xi\lambda$, from (18) and (19), we get

$$E < \frac{2\sqrt{2\hbar}}{p\pi}\left(\frac{\mathrm{e}^2}{4\pi\epsilon_0}\right)^{\frac{3}{4}} m^{-\frac{1}{4}}\xi^{-\frac{9}{4}}\lambda^{-\frac{5}{4}} \triangleq E_{\max}. \tag{20}$$

Substitute back to (17), we can take $\bar{n}_0 = \frac{k}{4}\frac{\epsilon_0\sigma_{\text{eff}}\lambda}{\mathrm{e}a_0}E_{\max}$ as the upper bound of $\bar{n}_{\text{eff}}$. It can be seen that

$$\bar{n}_0 = 6\times 10^7 k m^{-\frac{1}{4}}\xi^{-\frac{9}{4}}\lambda^{\frac{7}{4}}. \tag{21}$$

In the cases considered, it is suitable to limit $k \leqslant 2$, 9u $\leqslant m \leqslant$ 200u (u= 1.66057×10^{-27} kg). For $m = 9$u, $k = 2$, we get

$$\bar{n} = 3.4\times 10^{14}\xi^{-\frac{9}{4}}\lambda^{\frac{7}{4}}.$$

A large λ and a small ξ result in a large $\bar{n}$. When $\lambda = 10^{-6}$ m and $\xi = 2$, we obtain $\bar{n} = 2.3\times 10^3$.

Next, we assume that Steps 1 and 5 are implemented accurately and consider the limitation of the mean number of photons in Steps 2–4 in the CNOT gate. Using the method above, we can obtain the lower bound of failure probability. The result is that, when $\bar{n} = 10^4$ and the initial state is $|1\rangle_x|0\rangle_y$ or $|1\rangle_x|1\rangle_y$, after 10^2 times of CNOT operations, the failure probability reaches 10^{-2}. The failure probability under other initial states is relatively smaller, but not less than 10^{-4}. Then the average failure probability is estimated to be between 10^{-4} and 10^{-2}.

4.3 Permitted depth of logical operation

The threshold theorem in quantum computation declares that an arbitrarily long quantum computation can be performed reliably if the failure probability of each quantum gate is less than a critical value. The recognized threshold is 10^{-4} [24]. Knill [25] achieved a threshold of 10^{-2} using a numerical method, but it needs 10^6 physical qubits for one logical qubit, making it difficult to realize in practice. Aliferis et al. [41] gave a proof providing rigorous foundation for Knill's scheme and obtained a threshold of order 10^{-3}. Combining these thresholds with the failure probability from the laser field quantization discussion above, we can give an estimation of the permitted depth of the CNOT gate in the Cirac-Zoller QC scheme: The number of CNOT gates on the same pair of physical qubits is not more than 10^2 in one error-correction period, to ensure reliable implementation of the quantum computation.

In FTQC, the error between two successive error corrections is compared with the threshold. If the error is higher than the threshold, the computation cannot be reliably implemented. In the general case that there is encoding, decoding, and logical gates between two successive error corrections [24], for error-correction procedures such as encoding and decoding that are implemented in a fault-tolerant manner, the total number of physical CNOT gates on the same pair of physical qubits may be more than 10^2. Moreover, for complicated quantum algorithms such as Shor's algorithms, there may be more than one logical operation between two successive error corrections, then the number of physical CNOT gates on the same pair of physical qubits can further go beyond 10^2, which is larger than the value of permitted depth of logical operation derived. Furthermore, Liang and Yang [31] had illustrated that to obtain the maximum threshold, the operation executed between two successive error corrections could be bigger than 1, and the number of CNOT operations between two successive error-corrections was more likely to be larger than 10^2 for general quantum algorithms.

Besides studying whether quantum algorithms can run reliably on ion-trap QCs, we can also utilize the permitted depth of logical operation to design practical quantum algorithms, by carefully determining the maximum number of CNOT operations on the same pair of physical qubits between coding and decoding in one error-correction period.

5 Discussion

5.1 More accurate analysis

As illustrated earlier, based on the theory of concatenated codes and the threshold theorem for fault-tolerant quantum computation, the concatenating number k of FTQC should satisfy $\frac{(cp)^{2^k}}{c} \leqslant \frac{\epsilon}{p(n)}$ [24,30]. We can see that k is actually limited by the permitted depth of the logical operation discussed above, and a smaller k leads to a smaller $p_{\rm th}$, which results in a much smaller permitted depth of the logical operation. This is why we consider the result in Subsection 4.3 to be the upper bound of the permitted depth of the logical operation. The exact value can be obtained from (6).

The permitted depth of logical operation obtained above is only an estimation based on the ion-photon interaction cross-section calculated in Subsection 4.2, which is on foundation of [36] (Eq. (18) in page 533) and [37]. More accurate results are to be further explored. This is because the physical issue discussed herein is driving Rabi oscillation of bound states through scattering, which is related to both bound state theory and scattering theory in quantum mechanism. Treating this physical issue rigorously is a study without many existing results.

5.2 Results for the single-qubit gates

For single-qubit gates that form a universal gate set of quantum computation together with CNOT gates, we also evaluate the effect from quantum nature of the driving field. Some discussions have been made in [22], and the results obtained here are consistent with that in [22].

The Hamiltonian and unitary operator for single-qubit gates are just that given in (9) and (10), where phonons are not involved. Suppose we have an initial state of an ion qubit $|\psi(0)\rangle = \alpha|0\rangle + \beta|1\rangle$, where $|\alpha|^2 + |\beta|^2 = 1$. A single qubit gate is usually implemented through a $k\pi$ pulse in state $\sum_{n=0}^{\infty} c_n|n\rangle$ in the Cirac-Zoller scheme. After a $k\pi$ pulse, the reduced density matrix is $\rho^{(1)}$ [22], with

$$\begin{aligned}
\rho_{11}^{(1)} &= |\alpha|^2 s_4 + \frac{\mathrm{i}}{2}(\alpha\beta^* - \alpha^*\beta)\mathrm{e}^{\mathrm{i}\phi} s_2 + |\beta|^2(1 - s_6),\\
\rho_{12}^{(1)} &= \alpha\beta^* s_5 + \mathrm{i}(|\alpha|^2 \mathrm{e}^{\mathrm{i}\phi} s_1 - |\beta|^2 \mathrm{e}^{-\mathrm{i}\phi} s_7) + \alpha^*\beta s_3,\\
\rho_{21}^{(1)} &= \alpha^*\beta s_5 - \mathrm{i}(|\alpha|^2 \mathrm{e}^{\mathrm{i}\phi} s_1 - |\beta|^2 \mathrm{e}^{-\mathrm{i}\phi} s_7) + \alpha\beta^* s_3,\\
\rho_{22}^{(1)} &= |\alpha|^2(1 - s_4) - \frac{\mathrm{i}}{2}(\alpha\beta^* - \alpha^*\beta)\mathrm{e}^{\mathrm{i}\phi} s_2 + |\beta|^2 s_6,
\end{aligned}$$

where s_i $(i = 1, \ldots, 7)$ are summations similar to $\sum_{n=0}^{\infty} \frac{\mathrm{e}^{-\bar{n}}\bar{n}^n}{n!} f_{i0}(n, \bar{n}, k)$ in (15), which have been obtained in [22].

Consider the transform from $\rho^{(0)} = |\psi(0)\rangle\langle\psi(0)|$ to $\rho^{(1)}$. Using the natural representation of hyper-operators, we have

$$\overrightarrow{\rho^{(1)}} = Q\overrightarrow{\rho^{(0)}}, \tag{22}$$

where Q is a function of k, $\bar{n}$ (in s_i $(i = 1, \ldots, 7)$) and ϕ. Then we can obtain

$$Q(k, \phi, \bar{n}) = \begin{pmatrix}
s_4 & \frac{1}{2}\mathrm{i}\mathrm{e}^{\mathrm{i}\phi} s_2 & -\frac{1}{2}\mathrm{i}\mathrm{e}^{\mathrm{i}\phi} s_2 & 1 - s_6\\
\mathrm{i}\mathrm{e}^{\mathrm{i}\phi} s_1 & s_5 & s_3 & -\mathrm{i}\mathrm{e}^{-\mathrm{i}\phi} s_7\\
-\mathrm{i}\mathrm{e}^{\mathrm{i}\phi} s_1 & s_3 & s_5 & \mathrm{i}\mathrm{e}^{-\mathrm{i}\phi} s_7\\
1 - s_4 & -\frac{1}{2}\mathrm{i}\mathrm{e}^{\mathrm{i}\phi} s_2 & \frac{1}{2}\mathrm{i}\mathrm{e}^{\mathrm{i}\phi} s_2 & s_6
\end{pmatrix}.$$

Thus, for any single-qubit gate driven by repeated $k\pi$ pulses, we can obtain the operation result $\overrightarrow{\rho^{(j)}} = Q\overrightarrow{\rho^{(j-1)}} = \cdots = Q^j\overrightarrow{\rho^{(0)}}$, and for t different single-qubit gate successively applied to a qubit, the operation result can be

$$\vec{\rho} = Q(k_t, \phi_t, \bar{n}) \cdots Q(k_2, \phi_2, \bar{n}) Q(k_1, \phi_1, \bar{n}) \overrightarrow{\rho^{(0)}}.$$

The Hadamard and $\pi/8$ gates can be used to approximate any single-qubit gate to arbitrary accuracy [24]. The two gates are implemented using $\pi/2$ and π pulses, respectively. Similar calculation leads to a failure probability of 10^{-5} when $\bar{n} = 10^6$ and 10^2 $\pi/2$ or π pulses are applied. The mean number of photons here is not affected by the limit for sideband transition, but as pointed in [8], the implementation of the Cirac-Zoller CNOT gate needs sufficiently low laser intensities to only cause transition that modifies one of the collective normal modes of ions, then the effective mean number of photons and actual failure probability need further investigation.

5.3 Other related cases

Some cases exist that may lead to similar or different results. For the geometrical phase gate [26] and Mølmer-Sørensen gate [27] of ion-trap QCs, in which the laser field is also involved, similar results may be obtained. For the ion-trap QC driven by microwaves [42, 43], the results may be different because microwaves are more "classical" than lasers. The third case can involve other QC schemes driven by coherent fields. The results in this case need to be explored further.

6 Conclusion

We study the effect on ion-trap QCs from the quantum nature of the driving field and propose a theoretical limit (permitted depth of the logical operation) for ion-trap QCs that may impact the design of quantum

algorithms and realization of practical QCs. From the full-quantum theory of atom-field interaction, we provide an exact description of the Cirac-Zoller ion-trap QC system, and give for the first time its time evolution after many CNOT operations under the five steps of the Cirac-Zoller CNOT operation, to get the exact accumulated error in large-scale QCs.

Then, based on the algorithm which we developed in [22] to calculate a certain summation of trigonometric series with any given precision, and the natural (linear) representation of hyperoperators, we obtain the error probability after N CNOT operations with any given precision. The results showed that as the operation number increases, and the mean number of photons decreases, the failure probability after many CNOT operations increases. If the initial state was $|1\rangle_x|0\rangle_y$ or $|1\rangle_x|1\rangle_y$, the failure probability was relatively large. If the initial state was $|0\rangle_x|0\rangle_y$ or $|0\rangle_x|1\rangle_y$, the failure probability was relatively small.

Next, we obtained the theoretical limit (permitted depth of the logical operation) on the ion-trap QCs. After calculating the failure probability, considering the limitation to mean number of photons $\bar{n}$ [22], we arrived at the conclusion that the average failure probability was between 10^{-4} and 10^{-2} after 10^2 operations under general conditions. Combined with the threshold discussed in Subsection 4.3, we could give an estimation of the permitted depth of the logical operation for ion-trap quantum computation, i.e., the number of CNOT gates on the same pair of physical qubits is not more than 10^2 in one error-correction period, to ensure reliable implementation of the computation.

In addition to providing a more accurate physical model for the ion-trap quantum processor, we also overcame some mathematical difficulties. For example, the natural (linear) representation of operators was elaborately adopted to clearly show the transformation of one CNOT gate, building a solid base for later large-scale iterations to obtain the result after N CNOT operations in practical QCs. Based on the conclusion of this article, we can analyze whether quantum algorithms (such as Shor's factoring algorithm, discrete logarithm algorithm, and Grover's algorithm) can run reliably on ion-trap QCs or not, and practical quantum algorithms within theoretical limits can be designed.

Acknowledgements This work was supported by National Natural Science Foundation of China (Grant No. 61672517), National Cryptography Development Fund (Grant No. MMJJ20170108), National Key R&D Program of China (Grant No. 2016QY03D0503), and Beijing Municipal Science & Technology Commission (Grant No. Z191100007119006).

References

1 Shor P W. Algorithms for quantum computation: discrete logarithms and factoring. In: Proceedings of 35th Annual Symposium on Foundations of Computer Science, 1994. 124–134
2 Grover L K. A fast quantum mechanical algorithm for database search. In: Proceedings of the 28th Annual ACM Symposium on Theory of Computing, 1996. 212–219
3 Deutsch D, Jozsa R. Rapid solution of problems by quantum computation. In: Proceedings of the Royal Society of London A: Mathematical, Physical and Engineering Sciences, 1992. 553–558
4 Bernstein E, Vazirani U. Quantum complexity theory. SIAM J Comput, 1997, 26: 1411–1473
5 Simon D R. On the power of quantum computation. In: Proceedings of the 35th Annual Symposium on Foundations of Computer Science, 1994. 116–123
6 Rivest R L, Shamir A, Adleman L. A method for obtaining digital signatures and public-key cryptosystems. Commun ACM, 1978, 21: 120–126
7 Elgamal T. A public key cryptosystem and a signature scheme based on discrete logarithms. IEEE Trans Inform Theor, 1985, 31: 469–472
8 Cirac J I, Zoller P. Quantum computations with cold trapped ions. Phys Rev Lett, 1995, 74: 4091–4094
9 Linke N M, Maslov D, Roetteler M, et al. Experimental comparison of two quantum computing architectures. Proc Natl Acad Sci U S A, 2017, 114: 3305–3310
10 Monroe C, Raussendorf R, Ruthven A, et al. Large-scale modular quantum-computer architecture with atomic memory and photonic interconnects. Phys Rev A, 2014, 89: 022317
11 Piltz C, Sriarunothai T, Varón A F, et al. A trapped-ion-based quantum byte with 10(-5) next-neighbour cross-talk. Nat Commun, 2014, 5: 4679
12 Khromova A, Piltz C, Scharfenberger B, et al. Designer spin pseudomolecule implemented with trapped ions in a magnetic gradient. Phys Rev Lett, 2012, 108: 220502
13 Bowler R, Gaebler J, Lin Y, et al. Coherent diabatic ion transport and separation in a multizone trap array. Phys Rev Lett, 2012, 109: 080502
14 Pagano G, Hess P W, Kaplan H B, et al. Cryogenic trapped-ion system for large scale quantum simulation. Quantum Sci Tech, 2018, 41

15 Harty T P, Allcock D T C, Ballance C J, et al. High-fidelity preparation, gates, memory, and readout of a trapped-ion quantum bit. Phys Rev Lett, 2014, 113: 220501
16 Ballance C J, Harty T P, Linke N M, et al. High-fidelity quantum logic gates using trapped-ion hyperfine qubits. Phys Rev Lett, 2016, 117: 060504
17 Gaebler J P, Tan T R, Lin Y, et al. High-fidelity universal gate set for $^{9}Be^{+}$ ion qubits. Phys Rev Lett, 2016, 117: 060505
18 Leung P H, Landsman K A, Figgatt C, et al. Robust 2-qubit gates in a linear ion crystal using a frequency-modulated driving force. Phys Rev Lett, 2018, 120: 020501
19 Monz T, Nigg D, Martinez E A, et al. Realization of a scalable Shor algorithm. Science, 2016, 351: 1068–1070
20 Gea-Banacloche J. Some implications of the quantum nature of laser fields for quantum computations. Phys Rev A, 2002, 65: 022308
21 van Enk S J, Kimble H J. On the classical character of control fields in quantum information processing. Quantum Inf Comput, 2002, 21: 1–13
22 Yang L, Yang B Y, Chen Y F. Full quantum treatment of rabi oscillation driven by a pulse train and its application in ion-trap quantum computation. IEEE J Quantum Electron, 2013, 49: 641–651
23 Yang L, Chen Y F. A decoherent limit of fault-tolerant quantum computation driven by coherent fields. In: Proceedings of SPIE, 2007. 682708
24 Nielsen M A, Chuang I L. Quantum Computation and Quantum Information. Cambridge: Cambridge University Press, 2010
25 Knill E. Quantum computing with realistically noisy devices. Nature, 2005, 434: 39–44
26 Milburn G J, Schneider S, James D F. Ion trap quantum computing with warm ions. Fortschr Phys, 2000, 48: 801–810
27 Sørensen A, Mølmer K. Quantum computation with ions in thermal motion. Phys Rev Lett, 1999, 82: 1971–1974
28 Häffner H, Roos C F, Blatt R. Quantum computing with trapped ions. Phys Report, 2008, 4694: 155–203
29 Gruska J. Quantum Computing. New York: McGraw-Hill, 1999
30 Knill E, Laflamme R. Concatenated Quantum Codes. Technical Report, quant-ph/9608012. 1996
31 Liang M, Yang L. A note on threshold theorem of fault-tolerant quantum computation. 2010. ArXiv: 1006.4941
32 Watrous J. Theory of Quantum Information. Waterloo: University of Waterloo Fall, 2011
33 Luo X L, Zhu X W, Wu Y, et al. All-quantized Jaynes-Cummings interaction for a trapped ultracold ion. Phys Lett A, 1998, 237: 354–358
34 Mandel L, Wolf E. Optical Coherence and Quantum Optics. Cambridge: Cambridge University Press, 1995
35 Born M, Wolf E. Principles of Optics: Electromagnetic Theory of Propagation, Interference and Diffraction of Light. Cambridge: Cambridge University Press, 1999
36 Cohen-Tannoudji C, Dupont-Roc J, Grynberg G. Atom-Photon Interactions. New York: Wiley, 1992
37 Silberfarb A, Deutsch I H. Continuous measurement with traveling-wave probes. Phys Rev A, 2003, 68: 013817
38 Sargent M, Scully M O, Lamb W E. Laser Physics. New Jersey: Addison-Wesley, 1974
39 Wineland D J, Monroe C, Itano W M, et al. Experimental issues in coherent quantum-state manipulation of trapped atomic ions. J Res Natl Inst Stand Technol, 1998, 103: 259
40 Steane A. The ion trap quantum information processor. Appl Phys B, 1997, 64: 623
41 Aliferis P, Gottesman D, Preskill J. Accuracy threshold for postselected quantum computation. Qantum Inf Comput, 2008, 83: 181–244
42 Weidt S, Randall J, Webster S C, et al. Trapped-ion quantum logic with global radiation fields. Phys Rev Lett, 2016, 117: 220501
43 Lekitsch B, Weidt S, Fowler A G, et al. Blueprint for a microwave trapped ion quantum computer. Sci Adv, 2017, 3: e1601540